Theor Chem Acc (2002) 108:341–346
DOI 10.1007/s00214-002-0395-1

Theoretical Chemistry Accounts

Regular article

Ab initio study of rate constants of the reaction: HCN + OH → CN + H_2O

Chao Yang Wang[1], **Shaowen Zhang**[1], **Qian Shu Li**[1,2]

[1] School of Chemical Engineering & Material Science, Beijing Institute of Technology, Beijing 100081, China
[2] Institute of Theoretical Chemistry, State Key Laboratory of Theoretical and Computational Chemistry, Jilin University, Changchun 130023, China

Received: 18 August 2002 / Accepted: 30 August 2002 / Published online: 20 November 2002

Abstract. A method applying ab initio direct dynamics has been utilized in studying the hydrogen abstraction reaction HCN + OH → CN + H_2O. The geometries of the reactants, products, and the transition state have been optimized at the QCISD/6-311G(d, p) level. Single-point energies were further evaluated at the QCISD(T)/6-311 + G(2df, 2p)//QCISD/6-311G(d, p) level. The barrier heights for the forward and reverse reactions were predicted to be 15.95 and 7.51 kcal mol^{-1} at the QCISD(T)/6-311 + G(2df, 2p)//QCISD/6-311G(d, p) level, respectively. The reaction rate constants were calculated in the temperature range from 298 to 4,000 K using the canonical variational transition-state theory with a small-curvature tunneling correction. The results of the calculation show that the theoretical rate constants are in good agreement with experimental data over the measured temperature range of 400–2,600 K.

Key words: Ab initio direct dynamics – Canonical variational transition-state theory – Small-curvature tunneling – Rate constant – Hydrogen cynanide

1 Introduction

HCN is one of the main products of the decomposition process of nitramine propellants. Its subsequent oxidation, primarily by OH, is the initiator of the chemical reactions that ultimately govern the performance parameters of these propellants, such as the ignition delay and burning rates [1]. HCN has also been identified in fuel-rich hydrocarbon–air flames [1, 2, 3] and in hydrogen and hydrocarbon flames seeded with a variety of fuel-nitrogen compounds. Research results indicate that the oxidation of HCN by OH is an important path in the conversion of fuel-bound nitrogen to NO_x in hydrocarbon flames [3]. In the reaction zone, fuel nitrogen is rapidly converted to HCN [4, 5, 6, 7], while HCN is subsequently partially converted to CN. Since fuel-NO can be formed with either HCN or CN [6], it is important to know the rate constants of interconversion between HCN and CN. There is evidence that HCN is also a product of the biomass reaction, and after it is emitted into the troposphere and stratosphere [8], HCN keeps on reacting with many organic substances, such as CH_2O and CH_3OH, and is further changed to other harmful substances [9].

The rate constants for the reaction of HCN with OH have previously been investigated experimentally using different methods [10, 11, 12]. Woolgridge et al. [12] gave the rate constant expression of the forward reaction to be $k_{+1} = 3.90 \times 10^6 T^{1.83} \exp(-5{,}179/T)$ cm^3 mol^{-1} s^{-1} $= 6.48 \times 10^{-18} T^{1.83} \exp(-5{,}179/T)$ cm^3 $molecule^{-1}$ s^{-1}, in the temperature range from 500 to 2,000 K, by applying the narrow-line laser absorption technique. Jacobs et al. [11] obtained the forward and reverse reaction rate constant expressions to be $k_{+1} = (7.7 \pm 1) \times 10^{12} \exp[-(34.6 \pm 1)$ kJ$/RT]$ cm^3 mol^{-1} $s^{-1} = (1.3 \pm 0.2) \times 10^{-11}$ $\exp[-(4{,}163.66 \pm 120.34)/T]$ cm^3 $molecule^{-1}$ s^{-1} and $k_{-1} = (8.0 \pm 0.8) \times 10^{12}$ $\exp[-(31.2 \pm 0.6)$kJ$/RT]$ cm^3 mol^{-1} $s^{-1} = (1.3 \pm 0.1) \times 10^{-11}$ $\exp[-(3{,}754.5 \pm 72.2)/T]$ cm^3 $molecule^{-1}$ s^{-1}, respectively, within the temperature range from 518 to 1,027 K, with the laser-photolysis–laser-induced fluorescence technique. Szekely and et al. [10] determined the forward rate constant expression to be $K_{+1} = 2.41 \times 10^{-11} \exp(-5{,}500/T)$ cm^3 $molecule^{-1}$ s^{-1} in the temperature range from 850 to 2,600 K, and the reverse reaction rate constant expression to be $k_{-1} = 3.82 \times 10^{-11}$ $\exp(-6{,}700/T)$ cm^3 $molecule^{-1}$ s^{-1} in the temperature range from 850 to 2,600 K, with several experimental methods.

To our knowledge, however, only a few theoretical studies have been reported on the title reaction so far. Miller and Melius [13] studied the reaction potential surface of the reaction of HCN with OH at the BAC-MP4 level. Lin et al. [14] investigated the kinetic mechanisms of the reactions HCN + OH, HCN + O, and HCN + H. They gave the reaction path at the BAC-MP4

Correspondence to: Q. S. Li
e-mail: qsli@mh.bit.edu.cn

level. Xu et al. [15] calculated the theoretical rate constants for the hydrogen abstraction reaction of HCN with OH. They optimized the geometric parameters of the stationary points at the UHF/6-31G(d, p) level, and refined the single-point energies at the UMP2/6-31G(d, p) level. The minimum energy path (MEP) was obtained using intrinsic coordinates at the UHF/6-31G(d, p) level in the GAMESS program. They used the POLYRATE program to calculate the rate constants using the variational transition-state theory (TST) incorporating a tunneling correction. Their calculated rate constants were in agreement with the experimental rate constants obtained by Wooldbridge et al. [12] acquired in the temperature range from 1,312 to 1,491 K. In the present work, we investigated theoretically the dynamic properties of the hydrogen abstraction reaction with the more accurate theoretical method QCISD, in order to obtain the rate constants covering the temperature range of all known experimental results, 518–2,600 K.

2 Computational methods

2.1 Electronic calculations

The geometries of the reactants (HCN and OH), the transition state, and the products (CN and H2O) were optimized at the QCISD/6-311G(d, p) level. The gradients and Hessians of the stationary points were predicted at the same level. The energies of stationary points were refined at the QCISD(T)/6-311 + G(2df, 2p) level with the QCISD/6-311G(d, p) geometries. The MEP was obtained by the intrinsic reaction coordinate method with a gradient step size of 0.03 amu$^{1/2}$ bohr at the QCISD/6-311G(d, p) level. Then, at selected points along the MEP, the gradients and Hessians were calculated at the QCISD/6-311G(d, p) level. Because the shape of the potential surface near the transition state is very important for the computation of the rate constant, energies for the selected points along the MEP were also refined at the QCISD(T)/6-311 + G(2df, 2p) level.

2.2 Rate constants

The thermal rate constants at various temperatures were calculated using conventional TST and canonical variational TST (CVT) as implemented in the POLYRATE 8.2 program [16]. The CVT thermal rate constant for a gas-phase bimolecular reaction was determined by varying the location of the dividing surface along the reaction coordinate, s, to minimize the generalized TST rate constants, $k^{GT}(T,s)$ [17, 18, 19, 20]. Thus, the CVT thermal rate constant, k^{CVT}, at temperature T is given by

$$k^{\mathrm{CVT}}(T) = \min\{k^{\mathrm{GT}}(T,s)\} = \min\left\{\sigma\frac{k_{\mathrm{B}}T}{h}\frac{Q^{\mathrm{GT}}(T,s)}{Q^{\mathrm{R}}(T)}\exp[-V_{\mathrm{MEP}}(s)/k_{\mathrm{B}}T]\right\} ,$$

where Q^{GT} is the internal partition function of the generalized transition state; Q^R is the reactant partition function per unit volume; σ is the symmetry factor, which is 1 for the forward and 2 for the reverse direction of the HCN + OH → CN + H_2O reaction, and k_B and h are Boltzmann's and Plank's constants, respectively. Q^{GT} and Q^R are approximated as the products of electronic, rotational, and vibrational partition functions. For Q^{GT}, the relative translational partition function is also included. Translational and rotational partition functions were evaluated classically, whereas the vibrational partition functions were calculated quantum mechanically within the harmonic approximation.

Furthermore, the CVT rate constants were corrected with the small-curvature tunneling (SCT) [18, 19, 20, 21] transmission coefficient. The SCT transmission coefficients, which include the reaction-path curvature effect on the transmission probability, were based on the centrifugal-dominant small curvature semiclassical adiabatic ground-state approximation. In particular, the transmission probability at energy E is given by

$$P(E) = \frac{1}{\{1+\exp[-2\theta(E)]\}} ,$$

where $\theta(E)$ is the imaginary action integral evaluated along the reaction coordinate,

$$\theta(E) = \frac{2\pi}{h}\int_{s_1}^{s_r}\sqrt{2\mu_{\mathrm{eff}}(s)\left|E - V_{\mathrm{a}}^{\mathrm{G}}(s)\right|}\mathrm{d}s ,$$

and where the integration limits s_l and s_r are the reaction coordinate classical turning points. The effect of the reaction-path curvature on the tunneling probability is included in the effective reduced mass, μ_{eff}.

3 Results and discussion

3.1 Stationary points

The optimized geometric parameters of the reactants (HCN and OH), products (CN and H_2O), and their transition state are shown in Fig. 1. It is clearly seen that the computed geometric parameters of the reactants and

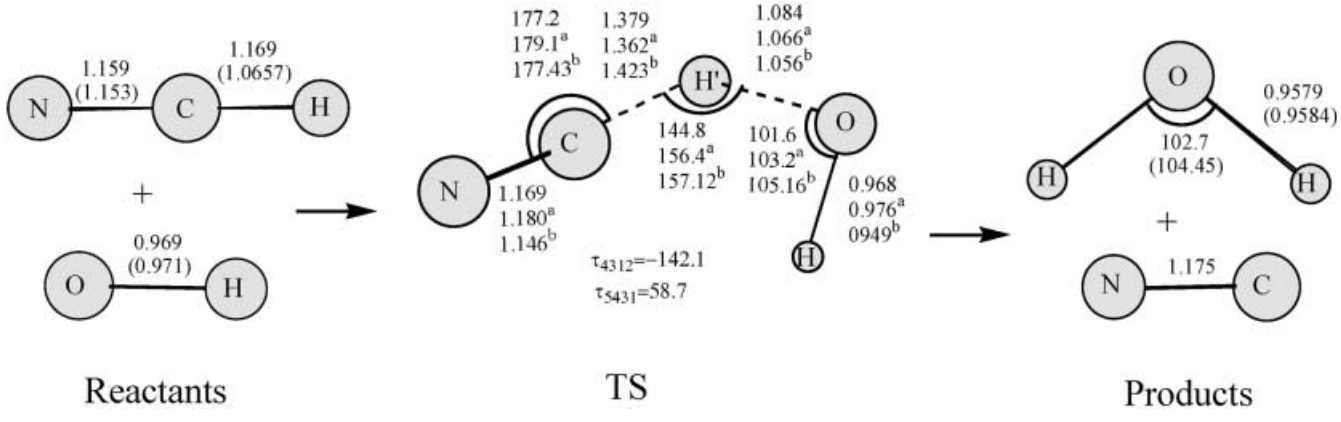

Fig. 1. Geometric parameters (in angstroms and degrees) of the stationary points at the QCISD/6-311G(d, p) level. The values in *parentheses* show experimental data [17]. τ: dihedral angle. The superscripts *a* and *b* indicate values from Ref. [21] and Ref. [22], respectively

products are in good agreement with the experimental data (given in parentheses) [22, 23]. The calculated structure of the transition state involved has C_1 symmetry. The bond angle of O–H′–C in the transition state is 144.8°. The C–H′ bond, which will to be broken as the reaction proceeds, is 0.31 Å longer than that in the free reactant HCN (Fig. 1). Simultaneously, the O–H′ bond, which will be formed as the reaction proceeds, is 0.132 Å longer than that in the free product H_2O. These values are in agreement with the results reported by Shapley and Bacskay [24] at the CASSCF(11/11)/cc-pVDZ level of theory, and Palma et al. [25] at the UHF/(TZ + P) level of theory except for the C–H′–O bond angle. In view of these structural characteristics, the transition state is seen to be more product-like. In fact, the experimental [26] and theoretical values of the reaction enthalpies are 6.18 ± 4.81 kcal mol^{-1} at 298 K and 8.44 kcal mol^{-1} at 0 K with the QCISD(T)/6-311 + G(2df, 2p)//QCISD/6-311G(d, p) method, respectively. This is reflected in the transition-state parameter L, defined as the ratio of the increase in the length of the C–H′ bond on breaking and the elongation of the O–H′ bond on its formation, each with respect to their equilibrium value in the reactant (HCN) and the product (H_2O) [27], respectively. $L = 2.35$ indicates that this reaction is an endothermic reaction.

The harmonic vibrational frequencies and zero-point energies of the reactants, products, and their transition state are listed in Table 1. It shows that the maximum error of the computed frequencies of the reactants and products is within 7% of the experimental values [28, 29, 30]. It can also be seen that the transition state possesses a large absolute value of the imaginary frequency (1,853 cm^{-1}), an result of the narrow barrier height and significant tunneling correction in the calculations of the rate constants. The calculated barrier heights are listed in Table 2. The theoretical barrier heights at the QCISD(T)/6-311 + G(2df, 2p)//QCISD/6-311G(d, p) level with zero-point energy corrections are 15.95 and 7.51 kcal mol^{-1}, respectively, for the forward and reverse reactions.

3.2 Reaction-path properties

The MEP was computed using the intrinsic reaction coordinate from the transition state to the reactants or to the products. The geometries, gradients and Hessians at selected points along the MEP were obtained at the QCISD/6-311G(d, p) level. The energies of selected points along the MEP were refined at the QCISD(T)/6-311 + G(2df, 2p) level to obtain more reasonable values.

The changes of the bond lengths of the species in the title reaction along the MEP are shown in Fig. 2. It is seen that the lengths of the C–H′ and O–H′ bonds change significantly near the transition state and that the lengths of other bonds change only slightly. As the reaction proceeds to products, the C–H′ bond length remains practically invariant until the intrinsic reaction coordinate reaches −0.75 amu$^{1/2}$ bohr, where it starts increasing almost linearly with increasing s. At the same time, the O–H′ bond length decreases almost linearly until the intrinsic reaction coordinate reaches 0.25 amu$^{1/2}$ bohr. During this process, the C–H′ bond breaks,

Table 2. Forward and reverse reaction potential barriers, E_b, with and without ZPE correction (kcal mol^{-1})

	QCISD/6-311G(d, p)		QCISD(T)/6-311 + G(2df,2p)	
	E_b	E_b + ZPE	E_b	E_b + ZPE
Forward	20.23	18.98	17.20	15.95
Reverse	11.79	9.41	8.76	6.38

[a] Ref. [10]
[b] Ref. [11]

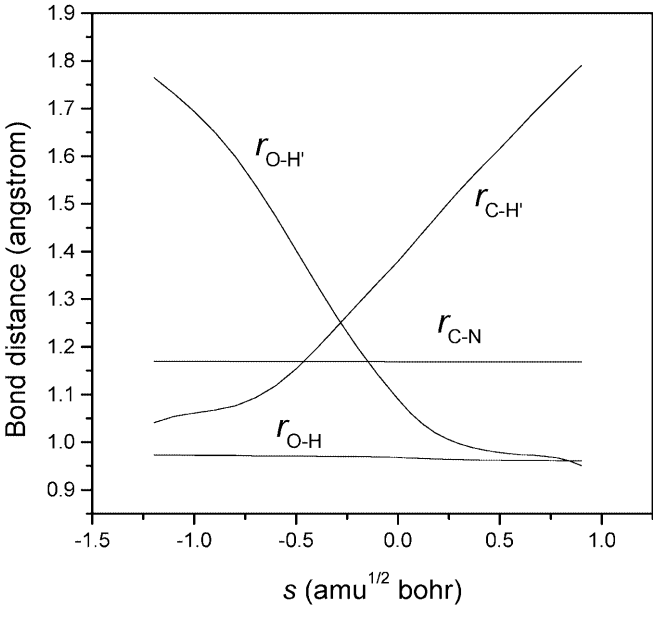

Fig. 2. Changes of bond lengths as functions of s at the QCISD/6-311G(d, p) level

Table 1. Harmonic vibrational frequencies and zero-point energies (ZPE) at the QCISD/6-311G(d, p) level

	Frequencies (cm^{-1})		ZPE (kcal mol^{-1})
	Theoretical	Experimental	
HCN	3,476 2,149 766 766	3,445 2,109 7,25[a]	10.23
OH	3,789	3,650[b]	5.42
CN	2154	2,260[b]	3.08
H_2O	3,996 3,902 1,687	3,650 3,650 1,475[c]	13.70
Transition state	3,825 2,221 1,553 1,141 624 362 187 158 1,853*i*		14.40

[a] Ref. [23]
[b] Ref. [24]
[c] Ref. [25]

while the O–H′ bond gradually forms. Figure 2 shows that the geometric change mainly takes place in the region from about $s = -0.75$ to $s = 0.50$ amu$^{1/2}$ bohr.

The harmonic vibrational frequencies along the MEP are shown in Fig. 3. For the reactants ($s = -\infty$), HCN + OH, only five vibrational modes are nonzero. Of these, modes 1 and 3 are the O–H and C–N stretching vibrations, which do not change throughout the whole reaction process. Mode 4 changes from the H′–C–N bend vibrational mode in the reactant HCN to the H′–O–H bend vibrational mode in the product H_2O. Mode 5 changes from the H′–C–N bend vibrational mode in the reactant to that of free rotation and its frequencies tend to be zero in the product. The lowest three frequencies, 6, 7, and 8, are the free rotation or translation modes. Their frequencies tend to be zero at the reactants or products and reach their maximum in the transition -tate zone. Mode 2, in which the frequencies dropped dramatically near the transition state, must be directly related to the reaction process. When $s < 0$, it is related to the C–H′ stretching mode, and when $s > 0$, it is related to the O–H′ stretching mode. This is called the ''reactive mode''. The region where the frequencies change dramatically is also shown in Fig. 2.

Curves for the classical potential energy, V_{MEP}, and the ground-state vibrationally adiabatic potential energy, V_a^G, along the MEP are shown in Fig. 4 as functions of the intrinsic reaction coordinate. The curves for V_{MEP} and V_a^G are actually very similar in shape, and the positions of the maximum value on the curves lie at nearly the same location at $s = 0$ amu $^{1/2}$ bohr. This indicates that the variational effect is slight in our computation of the rate constant. The peaks on both curves are rather sharp near $s = 0$ amu$^{1/2}$ bohr, and this indicates that the tunneling effect on the theoretical rate constants should be large. In order to further investigate the variational effect, the dynamical bottleneck properties of the reaction are listed in Table 3. This table shows that

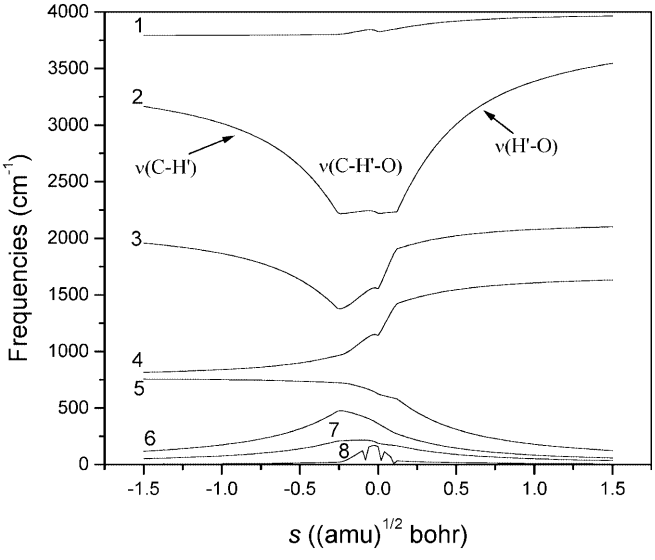

Fig. 3. Change of vibration frequency as functions of s at the QCISD/6-311G(d, p) level

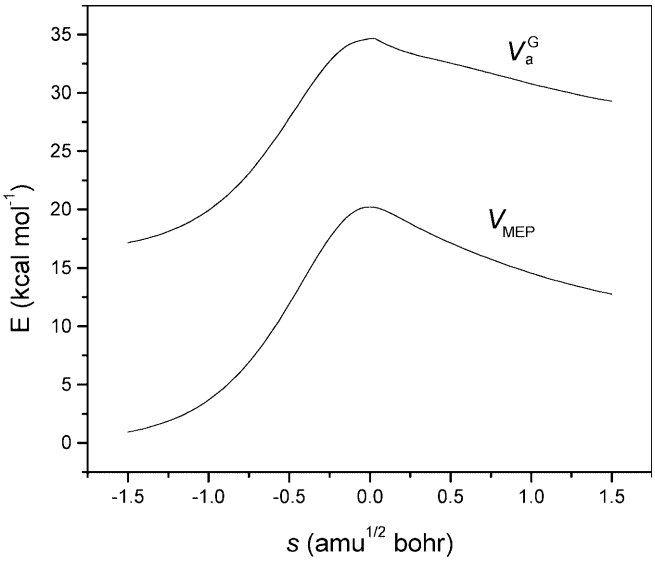

Fig. 4. Classical potential energy, V_{MEP}, and ground-state vibrationally adiabatic potential energy, V_a^G, as functions of s at the QCISD/6-311G(d, p) level

Table 3. Bottleneck properties determined using the transition-state theory (TST) and canonical variational TST (CVT) method

T (K)	s (bohr)	V_{MEP} (kcal)	V_a^G (kcal)
Saddle point[a]	0.000	15.95	30.35
0.00	−0.008	15.98	30.41
298.00	−0.008	15.98	30.41
400.00	−0.009	15.98	30.41
500.00	−0.009	15.98	30.41
600.00	−0.009	15.98	30.41
700.00	−0.009	15.98	30.41
1,000.00	−0.009	15.98	30.41
1,500.00	−0.010	15.98	30.41
2,000.00	−0.010	15.98	30.41
2,500.00	−0.010	15.98	30.41
3,000.00	−0.010	15.98	30.41
4,000.00	−0.010	15.98	30.41

[a] Conventional TST (other rows correspond to CVT)

the positions of the variational transition state at various temperatures deviate from the saddle point at $s = 0$ amu$^{1/2}$ bohr. The largest deviation is at 4,000 K, where $s = 0.0100$ amu$^{1/2}$ bohr, and the corresponding V_{MEP} and V_a^G are 15.98 and 30.41 kcal mol^{-1}, respectively. Since, for the conventional transition state ($s = 0$), V_{MEP} and V_a^G take the values 15.95 and 30.35 kcal mol^{-1}, respectively, the largest deviations, V_{MEP} $(s = -0.010) - V_{MEP}$ $(s = 0) =$ 0.03 kcal mol^{-1} and V_a^G $(s = -0.010) - V_a^G$ $(s = 0.0) =$ 0.06 kcal mol^{-1}, remain very small. This means that the variational corrections in the calculations of the rate constant are also very small.

3.3 Reaction rate constants

Curves of the TST, CVT, and CVT/SCT rate constants for the forward and reverse reaction as well as the

experimental values are plotted against the reciprocal of temperature in Fig. 5. Curves 1, 2, and 3 give the TST, CVT, and CVT/SCT rate constants, and curves 4, 5, and 6 give the experimental values. For the forward reaction in Fig. 5a, it can be seen that curve 3 is higher than curve 6, and it is lower than curves 4 and 5 in the whole temperature range. Curves 1 and 2 are far lower than curves 4 and 5, and they are closer to curve 6 in the whole temperature range. For the reverse reaction in Fig. 5b, curve 3 is always higher than curves 4 and 5, and about an order higher than the curve 4. So the difference of curve 3 from curve 4 is very large. From the two curves 4 in Fig. 5a and b, corresponding to the expressions [10] $k_{+1} = 2.41 \times 10^{-11} \times \exp(-5{,}500/T)$ and $k_{-1} = 3.82 \times 10^{-11} \times \exp(-6{,}700/T)$ cm^3 $molecule^{-1}$ s^{-1}, respectively, it can be seen that the rate constants of the forward reaction are larger than those of the reverse reaction, and that the effective activation energy of the forward reaction is less than that of the reverse reaction. However, since it is an endothermic reaction, it can be inferred that the rate constants of the forward reaction should be less than those of the reverse reaction. The results, however, are not in agreement, and our calculated results appear to be contrary to the expressions of the rate constants reported by Szekely et al. In addition, Table 4, which lists the theoretical and experimental reaction activation energies and rate constants, points further to this unexpected result.

It can also be observed in Fig. 5 that the TST and CVT rate constants (curves 1 and 2) are always very close to each other, indicating that the variational effect is very small in the calculation of the rate constant. Curves 1 and 2 are lower than curve 3 in the whole temperature range, and curves 1 and 2 have a different curvature from curve 3. This implies that the SCT corrections are necessary in the calculation of the reaction rate constant of this reaction. From the previous discussions, it can be predicted that the theoretical CVT/SCT rate constants might be more reliable.

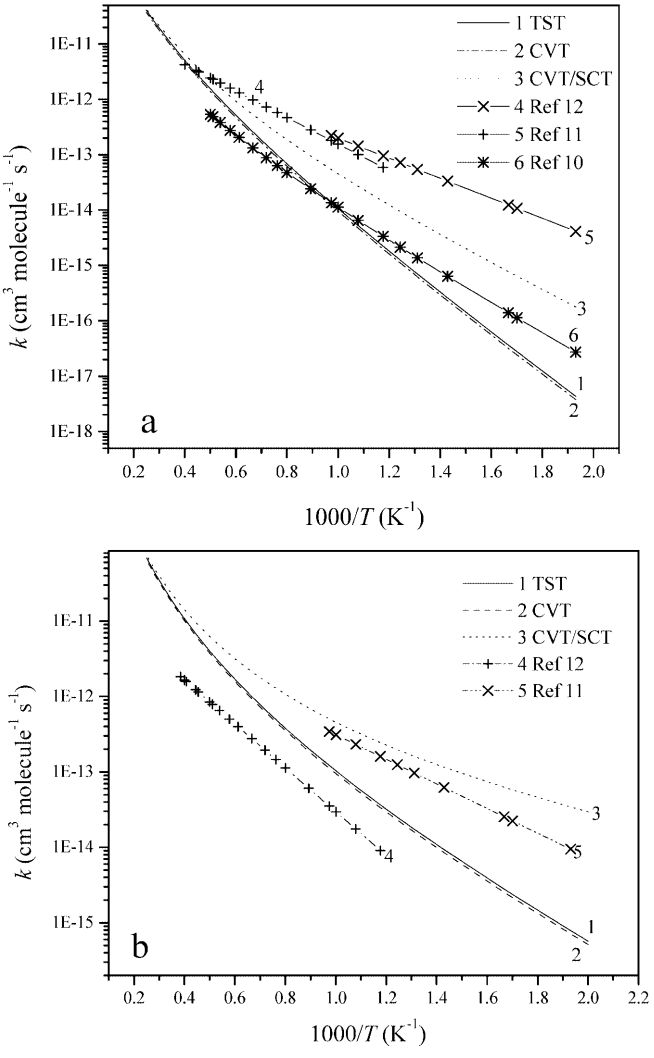

Fig. 5. a Forward reaction rate constants, k, as functions of the reciprocal of the temperature over the temperature range 500–4,000 K. **b** Reverse reaction rate constants as functions of the reciprocal of the temperature over the temperature range 500–4,000 K. *Curves 1*, *2*, and *3* are transition-state theory (TST), canonical variational TST (CVT) and CVT/small-curvature tunneling (SCT) rate constants, and *curves 4, 5* and *6* are experimental values, respectively

Table 4. Forward and reverse reaction rate constants (cm^3 $molecule^{-1}$ s^{-1}) at the QCISD(T)/6-311 + G(2df, 2p)//QCISD/6-311G (d, p) level in the temperature range 295–3,000 K

T	TST	CVT	CVT/ small-curvature tunneling	Experiment
Forward reaction rate constants				
298	6.98×10^{-23}	5.80×10^{-23}	1.14×10^{-19}	
400	4.93×10^{-20}	4.22×10^{-20}	8.67×10^{-18}	
500	2.49×10^{-18}	2.17×10^{-18}	1.22×10^{-16}	
600	3.64×10^{-17}	3.20×10^{-17}	7.75×10^{-16}	1.24×10^{-14}[a]
700	2.60×10^{-16}	2.30×10^{-16}	3.07×10^{-15}	3.34×10^{-14}[a]
850	2.23×10^{-15}	1.98×10^{-15}	1.43×10^{-14}	5.92×10^{-14}[b]
1,000	1.07×10^{-14}	9.54×10^{-15}	4.54×10^{-14}	1.56×10^{-13}[b]
1,250	6.90×10^{-14}	6.20×10^{-14}	1.88×10^{-13}	4.69×10^{-13}[b]
1,500	2.59×10^{-13}	2.34×10^{-13}	5.33×10^{-13}	9.77×10^{-13}[b]
1,730	6.57×10^{-13}	5.94×10^{-13}	1.13×10^{-12}	1.59×10^{-12}[b]
2,000	1.56×10^{-12}	1.41×10^{-12}	2.33×10^{-12}	2.44×10^{-12}[b]
2,250	2.98×10^{-12}	2.70×10^{-12}	4.06×10^{-12}	3.32×10^{-12}[b]
2,500	5.13×10^{-12}	4.65×10^{-12}	6.51×10^{-12}	4.23×10^{-12}[b]
3,000	1.22×10^{-11}	1.11×10^{-11}	1.41×10^{-11}	
3,500	2.38×10^{-11}	2.17×10^{-11}	2.59×10^{-11}	
4,000	4.09×10^{-11}	3.73×10^{-11}	4.28×10^{-11}	
Reverse reaction rate constants				
298	3.62×10^{-17}	3.01×10^{-17}	5.89×10^{-14}	
400	6.30×10^{-16}	5.39×10^{-16}	1.11×10^{-13}	
500	5.70×10^{-16}	5.15×10^{-16}	2.96×10^{-14}	
600	2.80×10^{-15}	2.54×10^{-15}	6.25×10^{-14}	2.55×10^{-14}[a]
700	9.33×10^{-15}	8.51×10^{-15}	1.15×10^{-13}	6.22×10^{-14}[a]
850	3.66×10^{-14}	3.36×10^{-14}	2.45×10^{-13}	9.09×10^{-15}[b]
1,000	1.03×10^{-13}	9.51×10^{-14}	4.56×10^{-13}	2.97×10^{-14}[b]
1,250	3.79×10^{-13}	3.54×10^{-13}	1.08×10^{-12}	1.14×10^{-13}[b]
1,500	1.00×10^{-12}	9.35×10^{-13}	2.14×10^{-12}	2.77×10^{-13}[b]
1,730	2.04×10^{-12}	1.91×10^{-12}	3.65×10^{-12}	5.01×10^{-13}[b]
2,000	4.04×10^{-12}	3.78×10^{-12}	6.26×10^{-12}	8.45×10^{-13}[b]
2,250	6.85×10^{-12}	6.42×10^{-12}	9.66×10^{-12}	1.23×10^{-12}[b]
2,500	1.08×10^{-11}	1.01×10^{-11}	1.42×10^{-11}	1.65×10^{-12}[b]

[a]Ref. [11]
[b]Ref. [10]

4 Summary

The geometric structures of the reactants (HCN and OH), products (CN and H_2O), and transition state of the title reaction have been optimized at the QCISD/6-311G(d, p) level, and the MEP taken was also calculated at the same level. The energies of the all stationary points and selected points along the MEP were refined at the QCISD(T)/6-311 + G(2df, 2p) level with the QCISD/6-311G(d, p) geometries. The dynamics of the hydrogen abstraction reaction were investigated using the POLYRATE 8.2 program. The forward and reverse rate constants were calculated on the basis of conventional TST and CVT with SCT corrections. The theoretical barriers of the forward and reverse reaction are 15.95 and 7.51 kcal mol^{-1}, respectively. The reaction enthalpy calculated with the QCISD(T)/6-311 + G(2df, 2p)//QCISD/6-311G(d, p) method is 8.44 kcal mol^{-1} at 0 K. Comparison of the theoretical rate constants with the experimental data shows that the CVT/SCT rate constants are reliable. The variational effect on the calculated rate constants is very small for this reaction. The SCT corrections play a very important role for the calculation of rate constants in the whole temperature region. These results imply that, in the low temperature range, the reaction HCN + OH → CN + H_2O is insignificant, but in the combustion process, this reaction becomes very important.

Acknowledgements. Our thanks are due to D.G. Truhlar for providing the POLYRATE 8.2 program. This work was supported by the National Science Foundation of China. We also thank D.C. Fang and Y. M. Xie for their valuable help, and P.R. Yan for reading our paper.

References

1. Melius CF (1987) In: Theoretical studies of the chemical reaction involved in the ignition of nitramines. Proceeding of the 24th JANAF combustion meeting. National Bureau of Standards, Washington, DC
2. Eberius KH (1973) In: 14th international symposium on combustion. The Combustion Institute, Pittsburgh, p 775
3. Miller JA, Bowman CT (1989) Prog Energy Combust Sci 15: 287
4. Haynes BS, Iverach D, Kirov NY (1975) In: 15th international symposium on combustion. The Combustion Institute, Pittsburgh, p 1103
5. Haynes BS (1976) Combust Flame 28: 113
6. Morley C (1976) Combust Flame 27: 189
7. Fenimore CP (1976) Combust Flame 26: 249
8. Lobert JM, Scharffe DH, Hao WM, Crutzen PJ (1990) Nature 346: 552
9. Murad E, Swider W, Moss RA, Toby S (1984) Geophys 11: 147
10. Szekely A, Hanson RK, Bowman CT (1984) Int J Chem Kinet 16: 1609
11. Jacobs A, Wahl M, Wellar R, Wolfrum J (1988) Chem Phys Lett 144: 203
12. Wooldridge ST, Hanson RK, Bowman CT (1995) Int J Chem Kinet 27: 1075
13. Miller JA, Melius CF (1986) In: 21st international symposium on combustion. The Combustion Institute, Pittsburgh, p 919
14. Lin MC, He Y, Melius F (1992) Int J Chem Kinet 24: 1103
15. Xu X-Z, Li Z-H, Liu R-Z (1997) Acta Physico-Chim Sin 13: 769 (in Chinese)
16. Chuang YY, Corchado JC, Fast PL, Villà J, Hu W-P, Liu Y-P Lynch GC, Jackels CF, Nguyen KA, Gu MZ, Rossi I, Isaacson EL, Truhlar DG (1999) Polyrate version 8.2. University of Minnesota, MN
17. Isaacson AD, Truhlar DG (1982) J Chem Phys 76: 1380
18. Truhlar DG, Isaacson AD, Skodje RT, Garrett BC (1982) J Phys Chem 86: 2252
19. Truhlar DG, Isaacson AD, Garret BC (1985) In: Baer M (ed) Theory of chemical reaction dynamics, vol 4. CRC, Boca Raton, FL, p 65
20. Steckler R, Hu W-P, Liu Y-P, Lynch GC, Garret BC, Isaacson AD, Melissas VS, Lu D-H, Troung TN, Rai SN, Hancock GC, Lauderdale JG, Joseph T, Truhlar DG (1995) Comput Phys Commun 88: 341
21. Liu Y-P, Lynch GC, Troung TN, Lu D-H, Truhlar DG, Garrett BC (1993) J Am Chem Soc 115: 2408
22. Lide DR (ed) (1992-1993) CRC handbook of chemistry and physics, 73rd edn. CRC Boca Raton, FL, Sect 9
23. Demaison J, Durbrulle A, Boucher D, Burie J, Typke V (1979) J Mol Spectosc 76: 1
24. Shapley WA, Bacskay GB (1999) J Phys Chem A 103: 4514
25. Palma A, Semprini E, Stefani F, Talamo A (1996) J Chem Phys 105: 5091
26. Atkison R, Baulch DL, Kerr JA, Rossi MJ, Troe J (1999) J Phys Chem Ref Data Suppl 28, Appendix 1
27. Louis F, Gonzalez C, Huie RE, Kurylo MJ (2000) J Phys Chem 104: 2931
28. King CM, Nixon ER (1968) J Phys Chem 48: 1685
29. Chase MW (1998) J Phys Chem Ref Data Monogr 9
30. Shimanouchi T (1972) NSRDS-NBS 39